

Structural properties of amorphous metal carbides; theory and experiment

Krisztina Kádas^{a,b}, Matilda Andersson^c, Erik Holmström^d, Heiko Wende^e, Olof Karis^f, Sigita Urbonaite^c, Sergei M. Butorin^f, Sergey Nikitenko^g, Kristina O. Kvashnina^g, Ulf Jansson^c, Olle Eriksson^{a,*}

^a*Division of Materials Theory, Department of Physics and Astronomy, Uppsala University, Box 516, SE-751 20, Uppsala, Sweden*

^b*Institute for Solid State Physics and Optics, Wigner Research Centre for Physics H-1525 Budapest, P.O.Box 49, Hungary*

^c*Department of Materials Chemistry, Uppsala University, Box 538, 751 21 Uppsala, Sweden*

^d*Instituto de Física, Facultad de Ciencias, Universidad Austral de Chile, Casilla 567, Valdivia, Chile*

^e*Universität Duisburg-Essen, Fakultät für Physik, Experimentalphysik, Lotharstr. 1, D-47048 Duisburg, Germany*

^f*Division of Molecular and Condensed Matter Physics, Department of Physics and Astronomy, Box 516 751 20 Uppsala, Sweden*

^g*European Synchrotron Radiation Facility, BP 220, 6 rue Horowitz, 38043 Grenoble, France*

Abstract

By means of theoretical modeling and experimental synthesis and characterization, we investigate the structural properties of amorphous Zr-Si-C. Two chemical compositions are selected, $\text{Zr}_{0.31}\text{Si}_{0.29}\text{C}_{0.40}$ and $\text{Zr}_{0.60}\text{Si}_{0.33}\text{C}_{0.07}$. The amorphous structures are generated in the theoretical part of our work, by the stochastic quenching (SQ) method, and detailed comparison is made as regards structure and density of the experimentally synthesized films. These films are analyzed experimentally using X-ray absorption spectroscopy, transmission electron microscopy and X-ray diffraction. Our results demonstrate for the first time a remarkable agreement between theory and experiment concerning bond distances and atomic coordination of this complex amorphous metal carbide. The demonstrated power of the SQ method opens up avenues for theoretical predictions of amorphous materials in general.

Keywords: Amorphous materials, Ab initio calculations, X-ray absorption spectroscopy, Metal carbide glasses, Atomic structure

*Corresponding author

Email address: `Olle.Eriksson@physics.uu.se` (Olle Eriksson)

1. Introduction

Deposition of thin films from the vapor phase may lead to amorphous structures. A group of materials which often exhibit non-crystalline structure is various transition metal-metalloid films such as Cr-C, Zr-Si, and Fe-B.[1–3] Interestingly, they are also important components in metallic glasses formed during rapid quenching from a melt, suggesting that the tendency to form amorphous structure is related to inherent properties of the elements and interactions between these elements. To obtain a more detailed understanding of the formation of amorphous structures and glasses we need to develop theoretical methods to model the structure and bonding in these non-crystalline environments. This can be achieved by e.g. molecular dynamics (MD) [4], Monte Carlo simulation [5], and reverse Monte Carlo simulation.[6] Unfortunately, these methods suffer from being computationally expensive or to rely on interatomic potentials with sometimes questionable accuracy. In this study we investigate another approach, namely the stochastic quenching (SQ) method,[7, 8] which combines computational efficiency and accuracy in describing the chemical interaction. In this method the atoms are placed randomly in the calculation cell, and then they are relaxed using first-principles density functional (DFT) calculations until the force on every atom is negligible. It has been shown that this way of generating amorphous structures is possible.[7, 8] However, the present investigation is the first in which a detailed comparison between experiment and the SQ theory is made in terms of structural properties, such as bond length and nearest neighbor coordination, in particular for a material with complex chemical interactions.

In this study, we have selected the Zr-Si-C system as an amorphous model system, since transition metal carbides and silicides are known to have complex chemistry, with competing metallic and covalent bonds.[9] We deposit amorphous films using magnetron sputtering from elemental targets and confirm the structure experimentally with several techniques. The choice of elements is based on several facts. First, Zr is a well-known base element in many metallic glasses. The atom has a large radius (1.59 Å), favorable for amorphous structure formation when combined with several other elements with smaller radii.[10] Second, the Zr-Si system is well-known to produce amorphous thin films with magnetron sputtering for potential use as e.g. diffusion barriers.[3] The addition of carbon to a ternary Zr-Si-C film

will create a multicomponent system with different atomic radii favorable for glass formation.[10] Also, in a ternary Zr-Si-C film a wide variety of bond types are formed (metallic Zr-Zr, and covalent Zr-C, Zr-Si and Si-C bonds), which makes it possible to create a network structure which should further favor an amorphous structure. The potential for applications in Zr-Si-C has recently been discussed.[11]

The paper is organized as follows. In Section 2, we describe the theoretical methods used in this study, and summarize the most important details of the calculations. The experimental methods are described in Section 3. The theoretical and experimental results are presented in Section 4.

2. Theory

The amorphous structures were generated in the theory by the stochastic quenching (SQ) method. This method is designed to describe amorphous structures in general, although there is less experience with it for complex materials with competing natures of the chemical binding. The amorphous structures are obtained by means of the following two steps of the SQ method: Firstly, the atoms are placed randomly in the calculation cell under the constraint that no pair of atoms are closer than a small value (typically 0.4 \AA). This constraint is required in order to avoid numerical problems in the first few steps in the calculation. Secondly, the positions are relaxed by means of a conjugate gradient method until the force on every atom is negligible. We found that the self averaging of 150-200 atoms usually properly describes the electronic properties at the thermodynamic limit. [8, 12–16] In the present study we used 200 atoms for most of the calculations, and made a few calculations with 400 atoms, for comparison.

The first-principles calculations were performed by means of the projector augmented wave [17, 18] method as implemented in the Vienna ab initio simulation package (VASP). [19–21]. This method is based on DFT. [22, 23] The exchange-correlation energy was calculated using the generalized gradient approximation with the Perdew, Burke, and Ernzerhof functional.[24] The calculations were considered converged when the potential energy difference between atomic iterations was less than 10^{-5} eV/atom , and the forces on each atom were typically less than 0.005 eV/\AA . A plane-wave energy cutoff of 400 eV was employed. The calculations were performed using only the Γ k-point.

3. Experimental

The Zr-Si-C film was deposited by non-reactive, unbalanced, DC magnetron sputtering in an ultra-high vacuum chamber (base pressure of 1×10^{-7} Pa). Separate 2 inch elemental targets (Kurt J. Lesker Ltd) with a purity of 99.999% for Si and C and 99.2-99.7% (grade 702) for Zr were used. The Ar plasma was generated at a constant pressure of 0.4 Pa with a deposition temperature of approximately 350 °C and bias of -50 V. All depositions were made using a rotating substrate holder to ensure a homogenous composition. Prior to deposition the Si and SiO₂ substrates were cleaned using ultrasonic bath in 2-propanol and ethanol for 5 minutes each and dried with nitrogen gas. The deposition rate was 40-70 Å/min depending on composition and the films for XRD, XPS and resistivity analysis was deposited with a thickness of ~ 0.3 μm. The chemical composition was analyzed by XPS using a Physical Systems Quantum 2000 spectrometer with monochromatic Al $K\alpha$ radiation and using sensitivity factors determined from binary reference samples of known composition. The crystallinity of the film was studied using XRD and TEM. The XRD analysis was made using a Siemens D5000 diffractometer and Cu $K\alpha$ radiation. A grazing incidence (GI) scan with an incidence angle of 1° was used to increase the signal from the thin film in relation to the substrate. For top view TEM the sample was prepared by depositing 40 nm thin film on a NaCl substrate. The NaCl was then dissolved in distilled water after deposition releasing the deposited film, which then was put on a carbon-coated copper grid and analyzed using a JEOL JEM-2100 operated at 200 kV. For the resistivity measurements each sample was measured six times and mean value and 95% confidence interval was calculated.

The XAS measurements were performed at BM26A (Dutch-Belgian beamline "DUBBLE") [25] of the European Synchrotron Radiation Facility (ESRF) in Grenoble, France. The incident energy was selected using the $\langle 111 \rangle$ reflection from a double Si crystal monochromator with bendable 2nd crystal for sagittal (horizontal) focusing. Vertical focusing and rejection of higher harmonics was achieved with Si mirror with Pt layer at an angle of 1.8 mrad relative to the incident beam. The incident X-ray beam had a flux of approximately 1×10^{11} photons/s on the sample position. The XAS data were measured in fluorescence mode by 9-element monolithic Ge detector [26] at Zr K edge (17988 eV) at room temperature. The Zr-Si-C

thin films on SiO₂ substrates were conventionally mounted on a thin tape. The energy calibration was performed on Zr foil. The data were recorded with a constant 0.05 Å⁻¹ step in k -space, in the energy range 17.75-18.85 keV. The intensity was normalised to the incident flux. The total energy resolution was estimated to be ~ 3.5 eV.

Spectra were analysed using the EXAFS implementation of IFEFFIT, ATHENA, and ARTEMIS. [27, 28] Model data were obtained from averages of many calculations of EXAFS data obtained from local structures present in the description of the amorphous material, using the FEFF software. [29–31]

4. Results and Discussion

On the experimental side, amorphous structures are typically generated by fast cooling from melts or with quenching of atoms during growth directly from the gas phase. Two films with composition Zr_{0.60}Si_{0.33}C_{0.07} and Zr_{0.31}Si_{0.29}C_{0.40} (according to our XPS analysis) were here deposited using magnetron sputtering. In our XRD measurements both films exhibited identical types of structure. Figure 1 shows the GI-XRD diffractograms of the Zr_{0.60}Si_{0.33}C_{0.07} and Zr_{0.31}Si_{0.29}C_{0.40} films. Two broad features, one at 36° and the other one at 60° is observed in the diffractogram. Another small peak is observed at 61° for the Zr_{0.60}Si_{0.33}C_{0.07} film, which is only a contribution from the Si(111) substrate. This type of diffractograms with only broad features is characteristic for an X-ray amorphous material, where these features are a consequence of the close-range order in the material. Fig. 2 shows the TEM image of the Zr_{0.60}Si_{0.33}C_{0.07} film. No indication of crystallinity is visible and the film shows a completely amorphous structure. Also, the energy filtered electron diffraction (inset) shows only broad, featureless rings without indication of any crystalline contribution. TEM and XRD together confirm that both films are amorphous.

The amorphous structures were generated in the theory by the SQ method. We calculated the energies of 50 stochastic structures of both compositions studied in the experiments, at different volumes, with supercells of 200 atoms (Fig. 3). We found an amorphous structure in all generated configurations. No partial crystallization or porosity was observed (Fig. 4). The calculated energies at constant V show roughly a Gaussian distribution for both compositions (insets in Fig. 3). We have determined the equilibrium volume (V_0) and bulk modulus (B_0) by fitting an exponential Morse-

type function to the average energies of Fig. 3, and obtained $V_0=13.72 \text{ \AA}^3/\text{atom}$ for $\text{Zr}_{0.31}\text{Si}_{0.29}\text{C}_{0.40}$, and $V_0=19.08 \text{ \AA}^3/\text{atom}$ for $\text{Zr}_{0.60}\text{Si}_{0.33}\text{C}_{0.07}$. Accordingly, our calculated equilibrium densities are $\rho_0=4.99 \text{ g/cm}^3$ for $\text{Zr}_{0.31}\text{Si}_{0.29}\text{C}_{0.40}$, and $\rho_0=5.64 \text{ g/cm}^3$ for $\text{Zr}_{0.60}\text{Si}_{0.33}\text{C}_{0.07}$. This is in line with the experimental densities of the corresponding binary crystalline phases: ZrC (6.730 g/cm^3 [32]), ZrSi_2 (4.883 g/cm^3 [33]), and Zr_5Si_3 (5.998 g/cm^3 [34]). We calculate $B_0=86 \text{ GPa}$ for $\text{Zr}_{0.31}\text{Si}_{0.29}\text{C}_{0.40}$, and $B_0=116 \text{ GPa}$ for $\text{Zr}_{0.60}\text{Si}_{0.33}\text{C}_{0.07}$. Within accuracy, B_0 in $\text{Zr}_{0.60}\text{Si}_{0.33}\text{C}_{0.07}$ is about the same as that in crystalline ZrSi_2 ($B_{\text{ZrSi}_2}=114.8 \text{ GPa}$ [35]), B_0 in $\text{Zr}_{0.31}\text{Si}_{0.29}\text{C}_{0.40}$, however, is noticeably lower than that. B_0 of both amorphous materials is smaller than that of crystalline Zr_5Si_3 ($B_{\text{Zr}_5\text{Si}_3}=152 \text{ GPa}$ [34]). As expected, the theoretical B of amorphous Zr-Si-C is significantly smaller than that of the crystalline carbides ($B_{\text{ZrC}}=223 \text{ GPa}$, $B_{\text{SiC}}=211 \text{ GPa}$).

We note that in amorphous materials, in contrast to crystalline materials, not only bond lengths can change upon compression, but also bond angles may vary, even to the extent that atoms may rearrange under compression. This invariably reduces the curvature of the energy versus volume relationship, when compared to a crystalline material with a reduced bulk modulus as the result. It is possible that this explains the much lower bulk modulus for amorphous $\text{Zr}_{0.31}\text{Si}_{0.29}\text{C}_{0.40}$ ($B_0=86 \text{ GPa}$) when compared to ZrC . The presence of Si also changes the bonding situation which may contribute to the relatively low bulk modulus of $\text{Zr}_{0.31}\text{Si}_{0.29}\text{C}_{0.40}$. It should also be mentioned here that the larger bulk modulus of $\text{Zr}_{0.60}\text{Si}_{0.33}\text{C}_{0.07}$ ($B_0=116 \text{ GPa}$) compared to that of $\text{Zr}_{0.31}\text{Si}_{0.29}\text{C}_{0.40}$ is somewhat surprising. The compound with more carbon has a higher density, and is expected to have more of strong Si-C bonds, which is expected to increase the bulk modulus, compared to a material with lower C content. Our calculations give the opposite trend. As we show in our study, the structures generated by the SQ method agree very well with observations. Hence it remains to be seen if the calculated trend in bulk modulus is a true effect, or possibly the result of the numerical treatment of the 50 configurations considered at each volume.

In order to compare the structural properties of the theoretical and experimental amorphous phases, in Fig. 5 and 6 we compare the simulated X-ray absorption fine structure (EXAFS at the Zr K-edge) signals of $\text{Zr}_{0.31}\text{Si}_{0.29}\text{C}_{0.40}$ and $\text{Zr}_{0.60}\text{Si}_{0.33}\text{C}_{0.07}$ to the experimental results. The simulations of the EXAFS spectra were performed

by means of real space multiple-scattering theory as implemented in the FEFF code [36]. The size of our cells prohibited the use of self-consistent potentials for the multiple scattering calculation of the X-ray absorption coefficients so we distributed overlapping atomic potentials on the sites in our amorphous 200 and 400 atom cells. The multiple scattering path expansion was used as the full multiple scattering approach loses accuracy at high k -values. In order to simulate periodic boundary conditions, we constructed a 3x3x3 supercell and calculated the normalized EXAFS signal $\chi_i^C(k)$ from each Zr atom in the center cell. The index i denotes individual Zr atoms, and the index C denotes individual 200 atom or 400 atom cells obtained by means of the SQ technique.

For each cell C , the calculated normalized EXAFS spectra from each individual Zr atom $\chi_i^C(k)$ were averaged to form the final $\chi^C(k)$. The theoretical spectra were calculated at 0 K and at room temperature by means of the correlated Debye model. The Debye temperature for the amorphous material is unknown, so we estimated a value of 600 K for the calculations that was close to the Debye temperatures of ZrC (614 K - 680 K [37, 38]), ZrSi₂ (495 K [39]), and Zr₅Si₃ (480 K [34]).

The theoretical curves of the 50 stochastic structures with 200 atoms (grey lines in Fig. 5 and 6) are very close to each other, especially in the small k region, and with increasing k they become more diffuse. We find that the overall agreement between the averages of the 50 individual structures (red lines) and the experimental signals (dashed black line) is good. In particular, we obtain excellent agreement between theory and experiment in the small k region. When comparing Fig. 5 and Fig. 6 we note that Fig. 6 reproduces observations almost perfectly, whereas a disagreement may be seen in Fig. 5 in the region of 6.5-7 Å⁻¹. We made a few additional calculations with 400 atoms per unit cell. As expected, due to the better statistics, the curves of the individual stochastic structures are closer to each other than for the 200 atom calculations [Fig. 5]. The average of the individual structures practically does not change compared to the 200 atom results, which clearly shows that a 200 atom unit cell is sufficient to describe amorphous Zr-Si-C.

Returning to the disagreement between theory and experiment in the region of 6.5-7 Å⁻¹, for the sample with low Zr concentration, it can be analyzed further by making a Fourier transformation of the data in Fig. 5. This transform (data not shown) shows that two bond lengths at distance just above 2.5 Å are located at 0.2

Å shorter distances in the theoretical data compared to the experiment. Although this may be viewed as a smaller error to an overall rather satisfactory agreement between experiment and theory, it can most likely be traced back to the very fast quenching of atomic coordinates in the SQ method, which is a somewhat slower process in the experimental samples. This may be realized by noting that for the low Zr concentration case, the two peaks for which the SQ method makes a 10 % error are associated to the average Zr-Zr and Zr-Si bond lengths. In this sample we expect few nearest neighbor Zr-Zr coordination, and a reduced amount of Zr-Si bonds, due to a preferred Zr-C bonding in combination with a rather large amount of C in the sample. However, an inspection of the simulated geometries gives that the SQ method does find a finite amount of Zr-Zr nearest neighbor coordination, due to the rapid quenching. For the sample with larger Zr concentration the amount of C is very low, and hence neither simulations nor experiment can exclude a nearest neighbor Zr-Zr coordination, resulting in a better agreement between theory and experiment for the EXAFS data.

To demonstrate that the agreement between theory and experiment is really due to an amorphous structure, we also calculated the EXAFS spectra of some known crystalline compounds of Zr, Si, and C (Fig. 7). In this EXAFS calculation we used the experimental crystal structures. The Debye temperatures used for these crystals were 680 K (ZrC) [38], 495 K (ZrSi₂) [39], 480 K (Zr₅Si₃) [34], and 600 K (Random alloy)[40]. The simulated EXAFS curves of these compounds do not agree at all with experiment. We also examined a case, where the calculated composition (Zr_{0.40}Si_{0.20}C_{0.40}) differs slightly from the experimental one (Zr_{0.43}Si_{0.30}C_{0.27}) to a small extent. For such a composition, the simulated curve does not agree with the experimental one, neither in the small, nor in the large k region (data not shown). This shows that both accurate structural information as well as precise chemical composition is needed to reproduce the experimental EXAFS data. The data in Figs. 5 and 6 are the first direct comparison on a structural level, between the SQ method and observations, and the agreement shows that a computationally efficient theory provides accurate atomic coordinates for a complex amorphous metal carbide.

In the following, we present additional structural details about amorphous Zr-Si-C. The theoretical average partial radial distribution functions (RDF) calculated for amorphous Zr_{0.31}Si_{0.29}C_{0.40} and Zr_{0.60}Si_{0.33}C_{0.07} (Figs. 8 and 9) show short range

order up to 6 Å for the C bonds (Zr-C, Si-C, and C-C), and up to 7-8 Å for the longer Zr-Zr, Zr-Si, and Si-Si bonds. In Table 1 the calculated average nearest neighbor distances are compared to distances in typical crystalline phases. Atoms are considered nearest neighbors (and also counted in the coordination numbers later), if they are closer than the first minimum in the corresponding partial RDF curves. We used the following cutoff distances for $Zr_{0.31}Si_{0.29}C_{0.40}$ (and $Zr_{0.60}Si_{0.33}C_{0.07}$): $d_{c,Zr-Zr}=4.11$ (4.29) Å, $d_{c,Zr-Si}=3.60$ (3.61) Å, $d_{c,Zr-C}=3.00$ (3.15) Å, $d_{c,Si-Si}=3.52$ (3.10) Å, $d_{c,Si-C}=2.33$ (2.41) Å, and $d_{c,C-C}=1.89$ (1.92) Å. For most pairs the distances are comparable to the corresponding crystalline bonds. The pairs with shorter bonds correlate with a reduced coordination of carbon. A lowered coordination means that the remaining bonds are stronger than in the crystalline phase. Such bond-shortening mechanism was observed in MAX phases.[41]

On the average, Zr atoms are coordinated by 15.4 atoms in $Zr_{0.31}Si_{0.29}C_{0.40}$, and by 14.9 atoms in $Zr_{0.60}Si_{0.33}C_{0.07}$ (Table 2). Both are larger than the coordination number in hexagonal close-packed (hcp) structure ($n_{hcp}=12$). Such high coordination is not unusual in amorphous structures.[42] Zr atoms are mostly coordinated by Zr atoms (Table 2 and Fig. 10a), which may be primarily due to their high concentration. Si atoms have a slight preference to have Zr neighbours (Fig. 10b), which is pronounced in $Zr_{0.60}Si_{0.33}C_{0.07}$, where the Zr-Si coordination is more than double that of the Si-Si coordination (Table 2), and Zr has almost ten times larger number of Si nearest neighbors than Si (see Table 3). Due to the small C content of amorphous $Zr_{0.60}Si_{0.33}C_{0.07}$, $n_{Zr,C}$, $n_{Si,C}$ and $n_{C,C}$ (defined in caption of Table 2) are well below one, and C atoms are mostly surrounded by Zr atoms (Fig. 10c). As expected, the number of C-C, Si-C and Zr-C bonds is significantly larger in $Zr_{0.31}Si_{0.29}C_{0.40}$ (Table 3). Here C atoms are mostly coordinated by Zr atoms, and on the average, each of them has at least one C nearest neighbors. Figure 10 shows that the structure can be described as a network structure of metal-metal, metal-carbide and metal-silicon bonds.

To examine the electronic structure of amorphous Zr-Si-C, we calculated their electronic density of states (DOS). Figure 11 shows the calculated the electronic density of states (DOS) of the representative structure of $Zr_{0.60}Si_{0.33}C_{0.07}$ at the equilibrium volume. The lowest lying states at around -12 eV originate from C 2s states, and mainly Si 3s orbitals contribute to states between -10.5 and -6 eV. The

large band between -5 and 0.6 eV is built up by Zr 4*d*, Si 3*p*, and C 2*p* states.

We calculate a large DOS at the Fermi level (E_F) for both compositions, i.e. that amorphous Zr-Si-C has a metallic character. This is in line with experimental observations: we measured $3.20 \pm 5 \mu\Omega\text{m}$ resistivity for $\text{Zr}_{0.60}\text{Si}_{0.33}\text{C}_{0.07}$, and $10.30 \pm 18 \mu\Omega\text{m}$ for $\text{Zr}_{0.31}\text{Si}_{0.29}\text{C}_{0.40}$. The states at E_F are dominated by Zr 4*d* orbitals, with some contribution from Si 3*p* and C 2*p* orbitals, i.e. amorphous Zr-Si-C is conducting, and the Zr *d* band has the most important role in electrical transport. In a simple approximation, the density of states at the Fermi level, $N(E_F)$, is directly related to the electrical conductivity. We calculate $N(E_F)=0.785$ states/eV/atom for amorphous $\text{Zr}_{0.60}\text{Si}_{0.33}\text{C}_{0.07}$, and $N(E_F)=0.353$ states/eV/atom for $\text{Zr}_{0.31}\text{Si}_{0.29}\text{C}_{0.40}$, suggesting that $\text{Zr}_{0.60}\text{Si}_{0.33}\text{C}_{0.07}$ has a higher conductivity. Indeed, we measured lower resistivity for $\text{Zr}_{0.60}\text{Si}_{0.33}\text{C}_{0.07}$ than for $\text{Zr}_{0.31}\text{Si}_{0.29}\text{C}_{0.40}$. We obtain higher DOS at E_F in amorphous $\text{Zr}_{0.60}\text{Si}_{0.33}\text{C}_{0.07}$ than that in crystalline MAX phases, e.g. in Ti_2SiC (0.36 states/eV/atom [41]), Ti_2GeC (0.43 states/eV/atom [43]), Zr_2InC (0.30 states/eV/atom [44]).

5. Conclusions

By means of the SQ method, we have generated structures for amorphous $\text{Zr}_{0.31}\text{Si}_{0.29}\text{C}_{0.40}$ and $\text{Zr}_{0.60}\text{Si}_{0.33}\text{C}_{0.07}$, and measured the EXAFS spectra, TEM and XRD diffractograms of samples with the same chemical composition. TEM and XRD confirm that both compositions are amorphous. We show that the calculated EXAFS spectrum is in excellent agreement with experiments, which serves as proof that theory reproduces accurately the structural properties of amorphous materials. This demonstrates for the first time that the SQ method provides reliable atomic coordinates of amorphous materials, even for very complex ternary systems, with competing chemical interactions, involving metallic and covalent bond-formation.[9] Our findings open up a new avenue to perform fast and accurate theoretical simulations for a wide class of amorphous materials.

Acknowledgements

The Swedish Research Council and the Swedish Foundation for Strategic Research (SSF, via the program Technical advancement through controlled tribofilms) are acknowledged for financial support. O.E. also acknowledges financial support

from VR, the KAW foundation, and the ERC (247062 - ASD). M.A. acknowledges financial support from SSF through the research program ProViking. E.H. would like to thank for support by FONDECYT grant 1110602. All computations made possible by a SNAC allocation, on supercomputer centra UPPMAX, NSC, and HPC2N.

References

- [1] Dehlinger A S, Pierson J F, Roman A, Bauer P. Surf Coat Techn 2003;174:331.
- [2] Ziebert C, Ye J, Stueber M, Ulrich S, Edinger M, Barzen I. Surf Coat Techn 2011;205:4844.
- [3] Wang Y, Cao F, Shao L, Ding M h. Thin Solid Films 2009;517:5593.
- [4] Thijssen J M. Computational Physics. Cambridge University Press, Cambridge, 1999. pp. 175.
- [5] Binder K, Heermann D W. Monte Carlo Simulation in Statistical Physics. Springer Series in Solid-State Sciences. Springer, Berlin ; Heidelberg ; New York, 1997.
- [6] McGreevy R L, Pusztai L. Mol Sim 1988;1:359.
- [7] Holmström E, Bock N, Peery T B, Lizárraga R, Lorenzi-Venneri G D, Chisolm E D, Wallace D C. Phys Rev B 2009;80:051111.
- [8] Holmström E, Bock N, Peery T, Chisolm E, Lizárraga R, Lorenzi-Venneri G D, Wallace D. Phys Rev B 2010;82:024203.
- [9] Gelatt C D, Williams A R, Moruzzi V L. Phys Rev B 1983;27:2005.
- [10] Inoue A, Takeuchi A. Acta Mat 2011;59:2243.
- [11] Krzanowski J E, Wormwood J. Surf Coat Technol 2006;201:2942.
- [12] Arhammar C, Pietzsch A, Bock N, Holmström E, Araujo C M, Grasjo J, Zhao S, Green S, Peery T, Hennies F, Amerioun S, Fohlich A, Schlappa J, Schmitt T, Strocov V N, Niklasson G A, Wallace D C, Rubensson J E, Johansson B, Ahuja R. Proc Natl Acad Sci USA 2011;108:6355.

- [13] Bock N, Holmström E, Peery T B, Lizárraga R, Chisolm E, Lorenzi-Venneri G D, Wallace D C. Phys Rev B 2010;82:144101.
- [14] Amézaga A, Holmström E, Lizárraga R, Menéndez-Proupin E, Bartolo-Pérez P, Giannozzi P. Phys Rev B 2010;81:014210.
- [15] Lizárraga R, Holmström E, Parker C, Arrouvel C. Phys Rev B 2011;83:094201.
- [16] Holmström E, Fransson J, Eriksson O, Lizárraga R, Sanyal B, Bhandary S, Katsnelson M I. Phys Rev B 2011;84:205414.
- [17] Blöchl P E. Phys Rev B 1994;50:17953.
- [18] Kresse G, Joubert D. Phys Rev B 1999;59:1758.
- [19] Kresse G, Hafner J. Phys Rev B 1993;47:558.
- [20] Kresse G, Furthmüller J. Comp Mat Sci 1996;6:15.
- [21] Kresse G, Furthmüller J. Phys Rev B 1996;54:11169.
- [22] Hohenberg P, Kohn W. Phys Rev 1964;136:B864.
- [23] Kohn W, Sham L. Phys Rev 1965;140:A1133.
- [24] Perdew J P, Burke K, Ernzerhof M. Phys Rev Lett 1996;77:3865.
- [25] Nikitenko S, Beale A M, van der Eerden A M J, MJacques S D, Leynaud O, O'Brien M G, Detollenaere D, Kaptein R, Weckhuysen B M, Bras W. J Synchrotron Radiat 2008;15:632.
- [26] Derbyshire G, Cheung K C, Sangsingkeow P, Hasnain S S. J Synchrotron Radiat 1999;6:62.
- [27] Ravel B, Newville M. Physica Scripta 2005;T115:1007.
- [28] Newville M. J Synchrotron Radiat 2001;8:322.
- [29] Zabinsky S I, Rehr J J, Ankudinov A, Albers R C, Eller M J. Phys Rev B 1995;52:2995.
- [30] Rehr J J, Albers R C, Zabinsky S I. Phys Rev Lett 1992;69:3397.

- [31] Mustre de Leon J, Rehr J J, Zabinsky S I, Albers R C. Phys Rev B 1991; 44:4146.
- [32] Martienssen W, Warlimont H. Springer Handbook of Condensed Matter and Materials Data. Springer, Berlin Heidelberg, 2005. Pp. 65., 114.
- [33] Zatorska G M, Dmytriv G S, Pavlyuk V V, Bartoszak-Adamska E, Jaskólski M. J Alloys Comp 2002;346:154.
- [34] Celis P B, Ishizaki K. J Mat Sci 1991;26:3497.
- [35] Peun T, Lauterjung J, Hinze E. Nucl Instr and Meth in Phys Res B 1995; 97:483.
- [36] Ankudinov A, Ravel B, Rehr J, Conradson S. Phys Rev B 1998;58.
- [37] Houska C R. J Phys Chem Solids 1964;25:359.
- [38] Lawson A C, Butt D P, Richardson J W, Li J. Phil Mag 2008;87:2507.
- [39] E McRae J S J F Mareche, Francois M. J Less Common Metals 1986;115:9.
- [40] The Debye temperature of the random substitutional alloy was estimated to be between the values for ZrC and Zr₅Si₃.
- [41] Palmquist J P, Li S, Persson P O A, Emmerlich J, Wilhelmsson O, Hogberg H, Katsnelson M I, Johansson B, Ahuja R, Eriksson O, Hultman L, Jansson U. Phys Rev B 2004;70:165401.
- [42] Egami T. J Non-Cryst Solids 2003;317:30.
- [43] Hug G. Phys Rev B 2006;74:184113.
- [44] He X, Bai Y, Li Y, Zhu C, Li M. Solid State Comm 2009;149:564.
- [45] Schachner H, Nowotny H N, Kudielka H. Monatshefte für Chemie 1954;85:1140.
- [46] Kwon Y U, Rzeznik M A, Guloy A, Corbett J D. Chem Mater 1990;2:546.

Figure captions

Figure 1: (Color online.) X-ray diffraction patterns for Zr-Si-C films with 7 at.% C (lower) and 40 at.% carbon (upper).

Figure 2: (Color online.) TEM micrographs of Zr-Si-C film with 7 at.% carbon.

Figure 3: (Color online.) Theoretical average energies (E_{av}) calculated for $Zr_{0.31}Si_{0.29}C_{0.40}$ (upper) and $Zr_{0.60}Si_{0.33}C_{0.07}$ (lower), as a function of the volume, V . In the insets the energy distribution of 50 stochastic configurations are shown at V_0 , where the energies were smeared by normalized Gaussian distributions with standard deviation of 0.01 eV.

Figure 4: (Color online.) One stochastic structure of amorphous $Zr_{0.60}Si_{0.33}C_{0.07}$, calculated at the equilibrium volume, having a total energy closest to the average energy of 50 structures of the same volume (representative structure). Zr, Si, and C atoms are displayed by silver, yellow, and cyan, respectively. For clear representation of the structure, bonds are not displayed in the figure.

Figure 5: (Color online.) The simulated (grey lines) and experimental (dashed lines) EXAFS signals of amorphous $Zr_{0.31}Si_{0.29}C_{0.40}$ (in arbitrary units). The averages over 50 individual configurations for the 200 atom case (upper) and over 5 configurations for the 400 atom case (lower) are shown by red lines.

Figure 6: (Color online.) The simulated (grey lines) and experimental (dashed line) EXAFS signals of amorphous $Zr_{0.60}Si_{0.33}C_{0.07}$ (in arbitrary units). The average of all simulated cells are shown by the red line.

Figure 7: (Color online.) Simulated EXAFS signals (in arbitrary units) for some crystalline compounds compared to the measured spectrum of amorphous $Zr_{0.31}Si_{0.29}C_{0.40}$. The crystalline alloy is a random substitutional alloy with the same composition as the amorphous alloy distributed on a NaCl-type crystal lattice with lattice constant $a=4.698$ Å.

Figure 8: (Color online.) Average partial radial distribution functions calculated for amorphous $Zr_{0.31}Si_{0.29}C_{0.40}$. The supercell size in the calculation was 200 atoms.

Figure 9: (Color online.) Average partial radial distribution functions calculated for amorphous $Zr_{0.60}Si_{0.33}C_{0.07}$. The supercell size in the calculation was 200 atoms.

Figure 10: (Color online.) Examples of calculated local structures around Zr (a), Si (b), and C (c) atoms in amorphous $\text{Zr}_{0.60}\text{Si}_{0.33}\text{C}_{0.07}$. Zr, Si, and C atoms are displayed by silver, yellow, and cyan, respectively.

Figure 11: (Color online.) Electronic density of states (in arbitrary units), calculated for the representative structure of amorphous $\text{Zr}_{0.60}\text{Si}_{0.33}\text{C}_{0.07}$ at the equilibrium volume. The top panel shows the total DOS of the 200 atom structure. The partial s , p , and d DOS curves are averages calculated for the different atom types. The Fermi level (E_{F}) is denoted by vertical dashed line.

Table 1: Average nearest neighbor distances ($d_{\text{TypeI}-\text{TypeII}}$ in Å) calculated for amorphous $\text{Zr}_{0.31}\text{Si}_{0.29}\text{C}_{0.40}$ and $\text{Zr}_{0.60}\text{Si}_{0.33}\text{C}_{0.07}$. For comparison, the distances in the corresponding crystalline materials are also listed.

	$\text{Zr}_{0.31}\text{Si}_{0.29}\text{C}_{0.40}$	$\text{Zr}_{0.60}\text{Si}_{0.33}\text{C}_{0.07}$	Crystalline
Zr-Zr	3.22	3.18	3.179 ^a
Zr-Si	2.75	2.75	2.724 ^b , 2.723 ^c
Zr-C	2.32	2.28	2.349 ^d
Si-Si	2.41	2.45	2.352 ^e
Si-C	1.86	1.89	1.887 ^f
C-C	1.41	1.41	1.545 ^g , 1.42 ^h

^a: in Zr of hexagonal $P6_3/mmc$ structure [32]

^b: in ZrSi_2 of $Cmcm$ structure [45]

^c: in Zr_5Si_3 of $P6_3/mcm$ structure [46]

^d: in ZrC of NaCl structure [32]

^e: in Si of diamond structure [32]

^f: in SiC of $F\bar{4}3m$ structure [32]

^g: in diamond [32]

^h: in graphene [32]

Table 2: Calculated average coordination numbers of 50 stochastic structures for amorphous $\text{Zr}_{0.31}\text{Si}_{0.29}\text{C}_{0.40}$ and $\text{Zr}_{0.60}\text{Si}_{0.33}\text{C}_{0.07}$. TypeI atoms (in rows) are coordinated by $n_{\text{TypeI,TypeII}}$ number of TypeII atoms (in columns) on the average.

	$\text{Zr}_{0.31}\text{Si}_{0.29}\text{C}_{0.40}$			$\text{Zr}_{0.60}\text{Si}_{0.33}\text{C}_{0.07}$		
	Zr	Si	C	Zr	Si	C
Zr	6.6	4.6	4.2	10.2	4.1	0.6
Si	4.9	3.6	1.6	7.4	1.5	0.2
C	3.3	1.1	1.1	5.2	0.9	0.1

Table 3: Calculated minimal (m_{\min}), maximal (m_{\max}) and average (m_{average}) number of nearest neighbors in amorphous $\text{Zr}_{0.31}\text{Si}_{0.29}\text{C}_{0.40}$ and $\text{Zr}_{0.60}\text{Si}_{0.33}\text{C}_{0.07}$. Numbers in parentheses give the percentages of the total number of nearest neighbors, where the minimal and maximal values are calculated for the corresponding individual stochastic structures.

	$\text{Zr}_{31}\text{Si}_{29}\text{C}_{40}$			$\text{Zr}_{60}\text{Si}_{33}\text{C}_7$		
	m_{\min}	m_{\max}	m_{average}	m_{\min}	m_{\max}	m_{average}
Zr-Zr	191 (19.4)	217 (22.2)	204.4 (20.7)	597 (48.5)	623 (50.7)	612.7 (49.4)
Zr-Si	258 (26.1)	305 (30.8)	285.1 (28.8)	467 (38.0)	511 (41.0)	490.2 (39.6)
Zr-C	235 (23.9)	282 (27.9)	260.7 (26.4)	59 (4.8)	78 (6.3)	72.0 (5.8)
Si-Si	90 (9.1)	120 (12.3)	104.0 (10.5)	38 (3.1)	64 (5.2)	50.2 (4.1)
Si-C	77 (7.7)	108 (10.8)	90.7 (9.2)	7 (0.6)	20 (1.6)	13.2 (1.1)
C-C	34 (3.4)	57 (5.9)	44.0 (4.5)	0 (0.0)	4 (0.3)	0.9 (0.1)

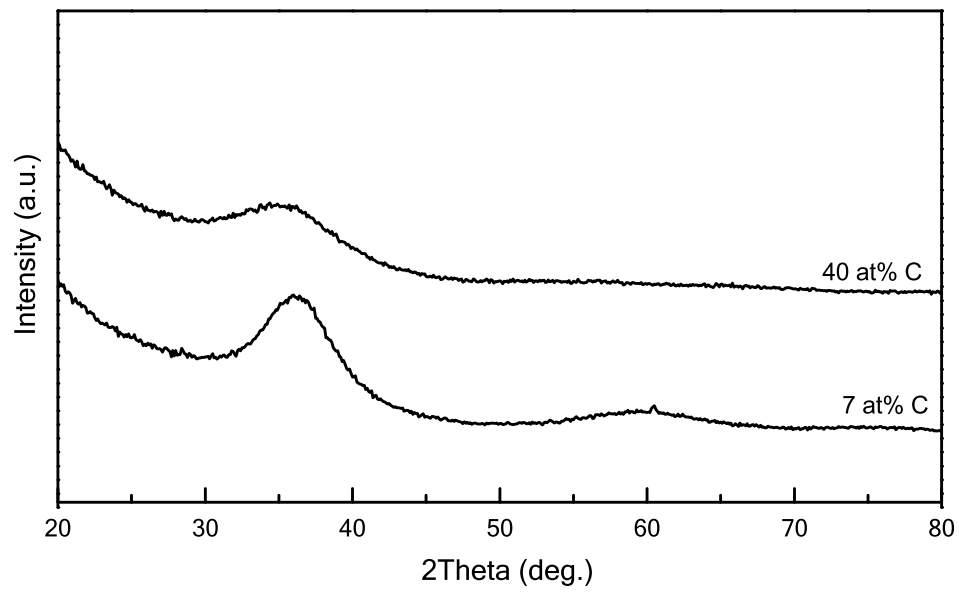


Figure 1

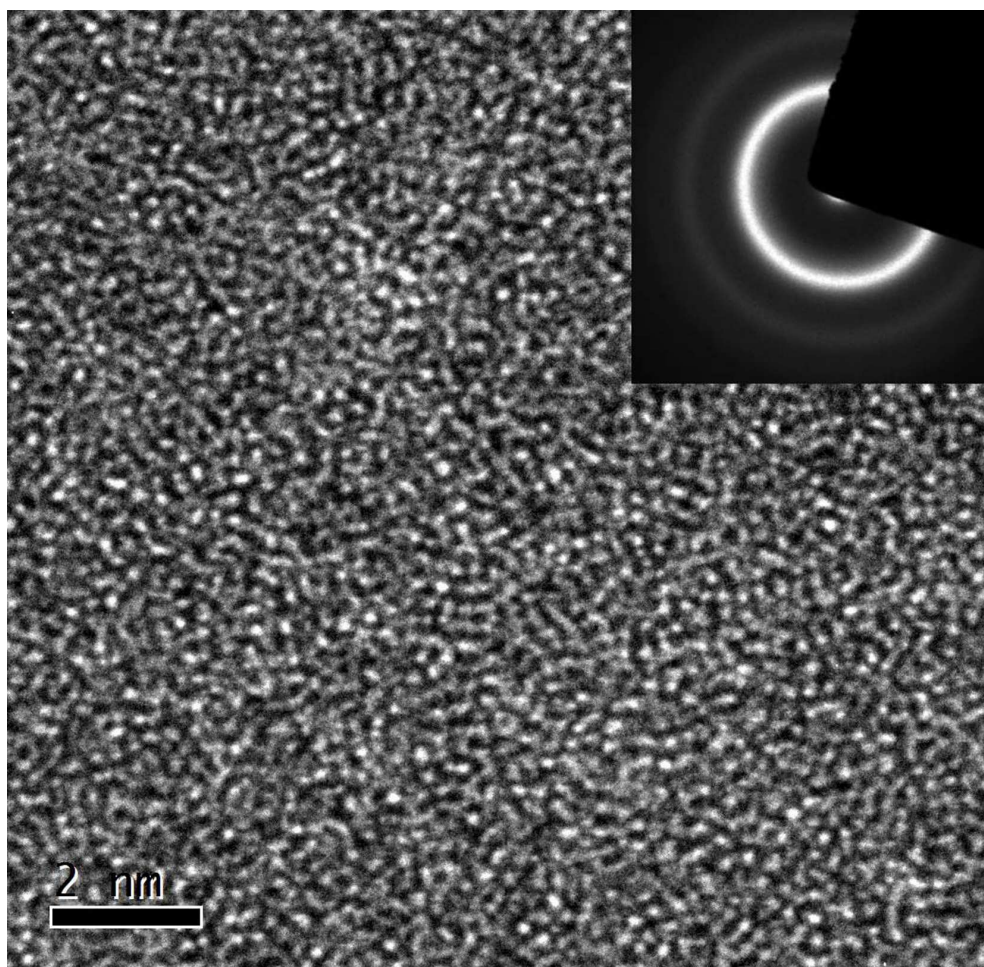


Figure 2

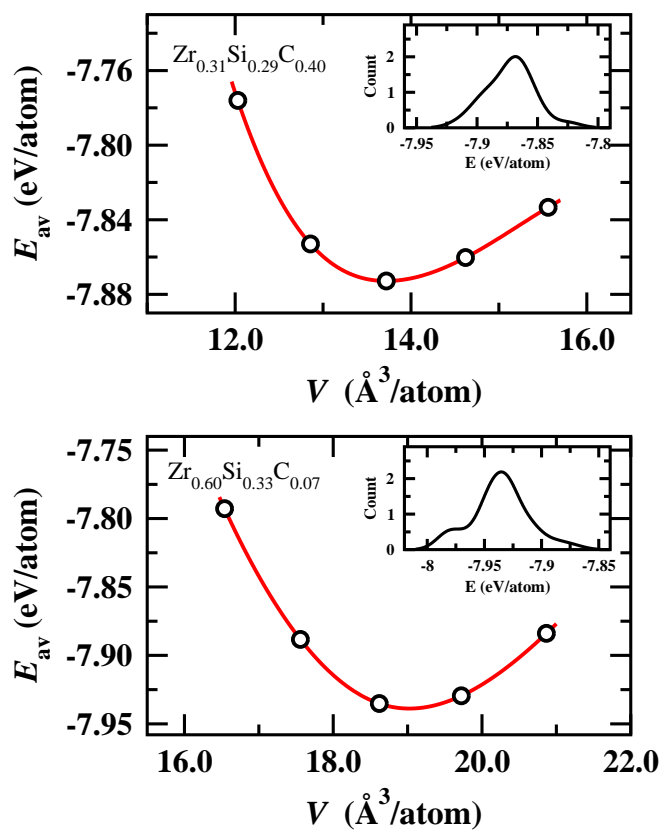


Figure 3

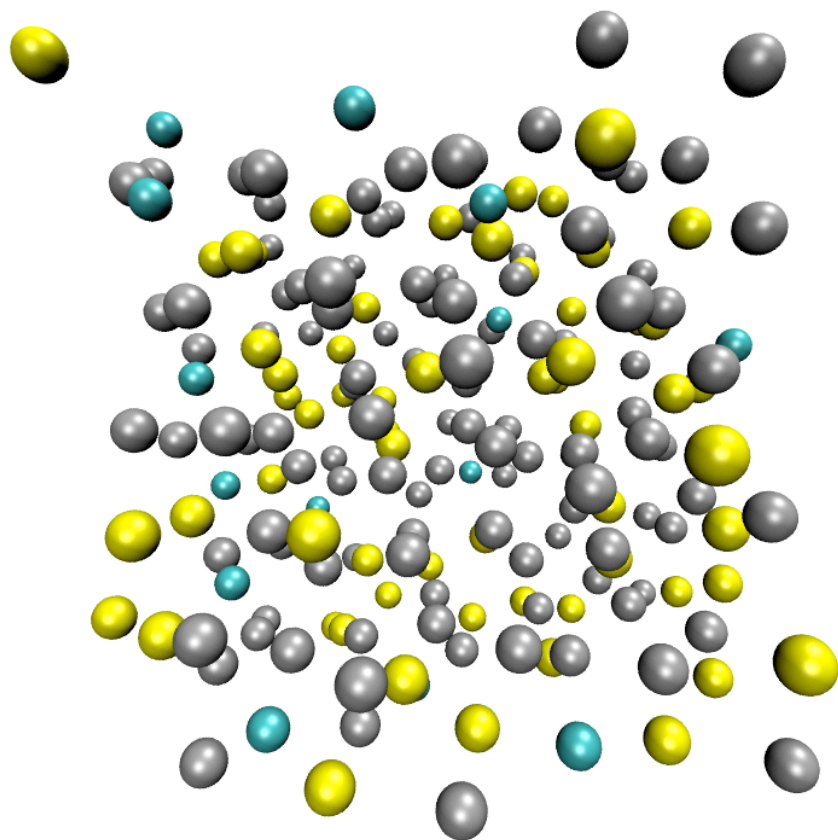


Figure 4

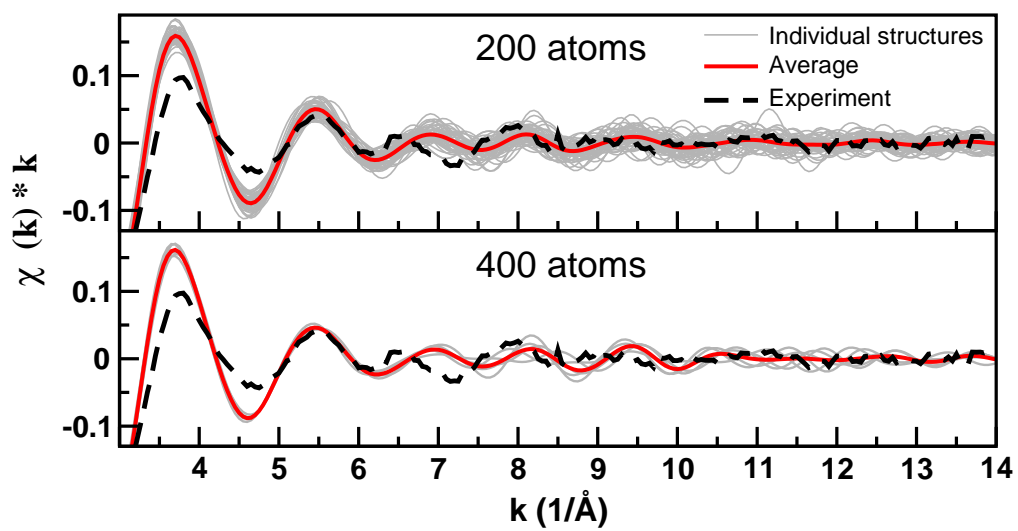


Figure 5

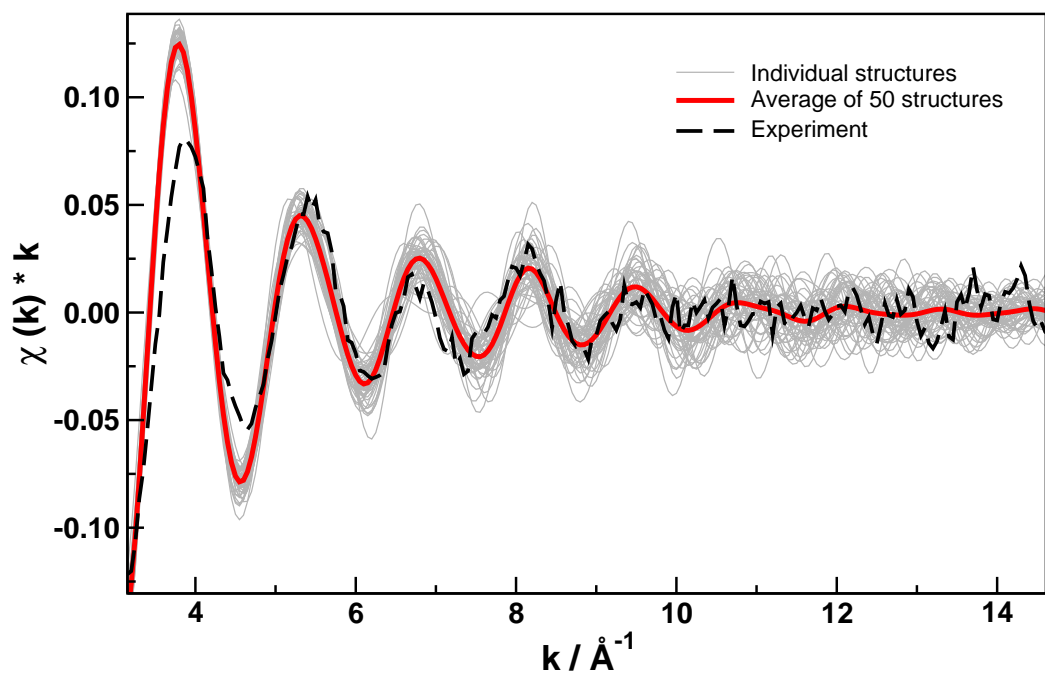


Figure 6

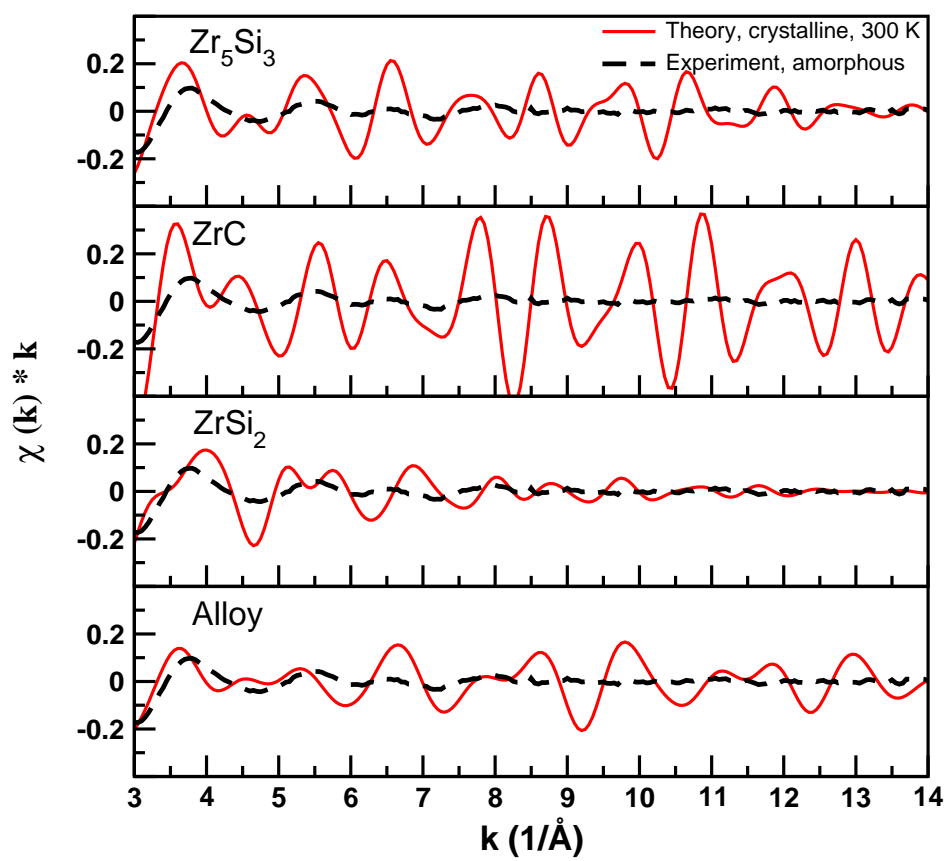


Figure 7

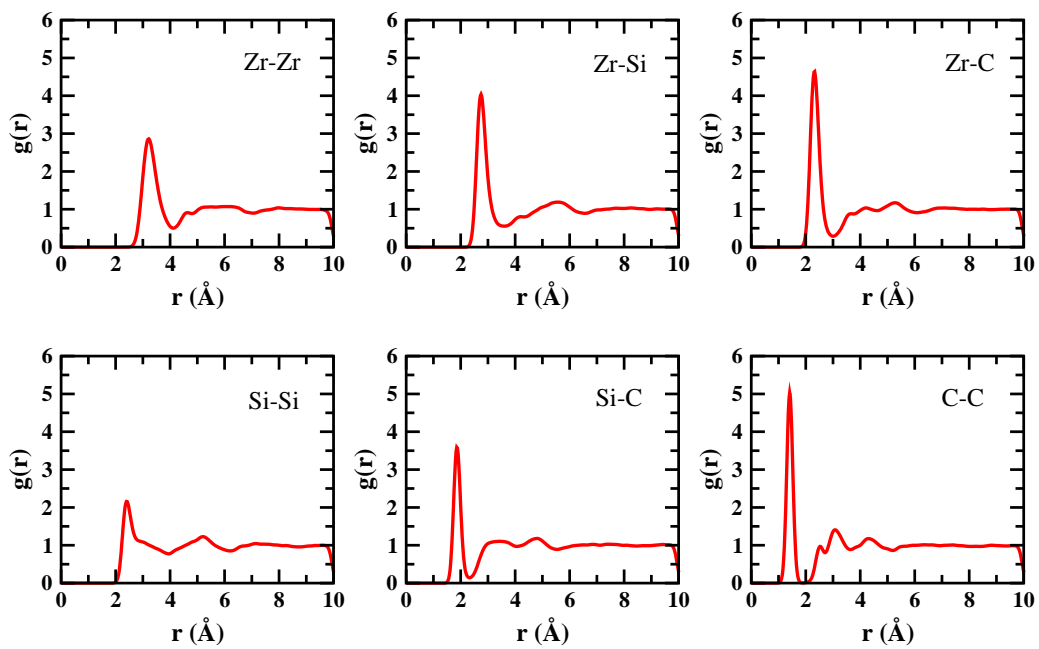


Figure 8

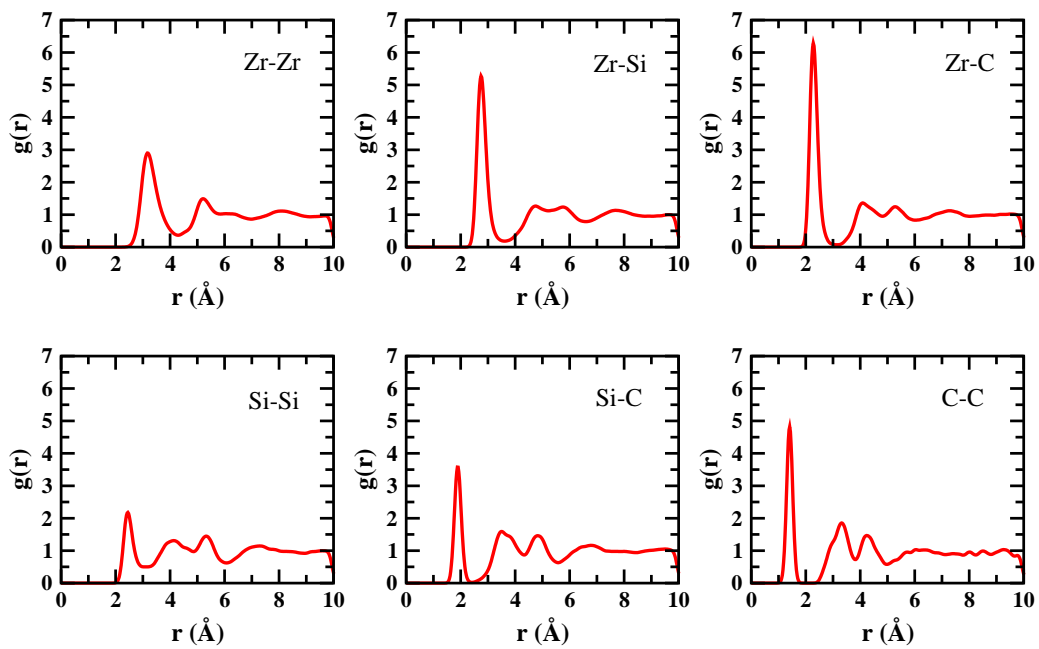


Figure 9

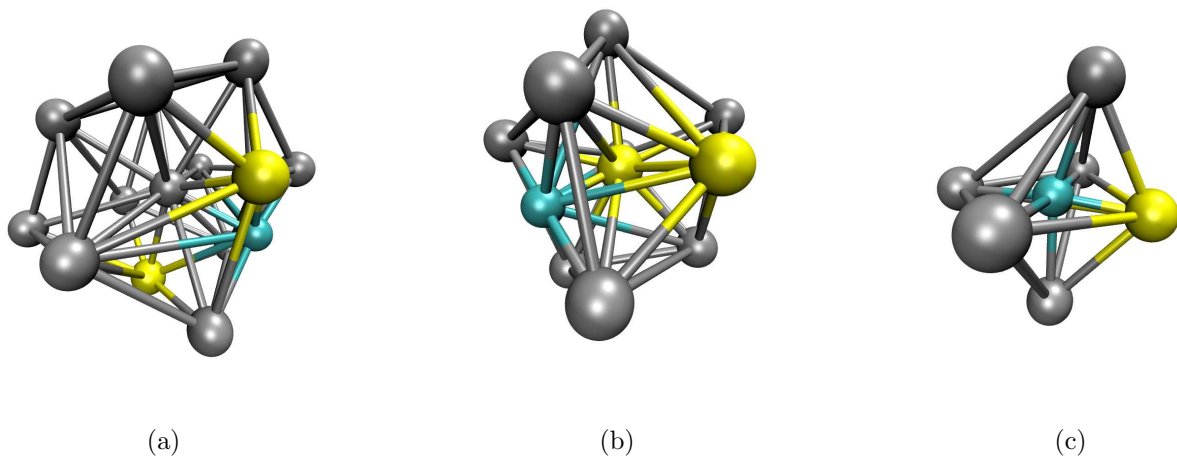


Figure 10

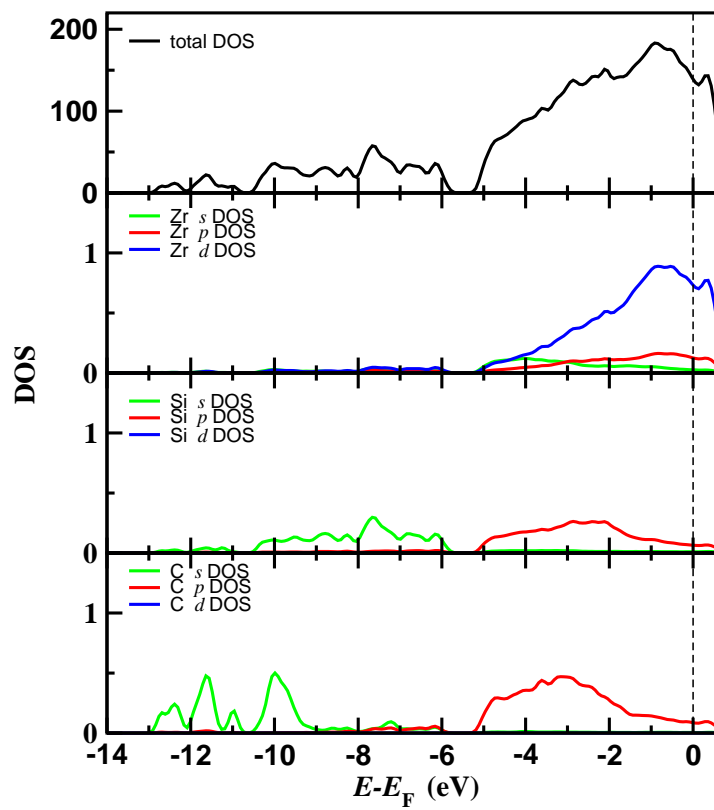


Figure 11